Received: 14 July 2023 | Revised: 15 September 2023 | Accepted: 24 October 2023

DOI: 10.4218/etrij.2023-0274

ORIGINAL ARTICLE

ETRI Journal WILEY

Multistage interference cancellation for cyclic interleaved frequency division multiplexing

G. Anuthirsha | **S. Lenty Stuwart**

Electronics and Communication Engineering, University College of Engineering, Nagercoil, Tamil Nadu, India

Correspondence
S. Lenty Stuwart, Electronics and Communication Engineering, University College of Engineering, Nagercoil, Tamil Nadu, India.
Email: lenty_s@yahoo.com

Funding information
Science and Engineering Research Board of the Department of Science and Technology, Government of India, Grant/Award Number: ECR/2017/001188

Abstract

Cyclic interleaved frequency division multiplexing (CIFDM), a variant of IFDM, has recently been proposed. While CIFDM employs cyclic interleaving at the transmitter to make multipath components resolvable at the receiver, the current approach of matched filtering followed by multipath combining does not fully exploit the diversity available. This is primarily because the correlation residues among the codes have a significant impact on multipath resolution. As a solution, we introduce a novel multipath successive interference cancellation (SIC) technique for CIFDM, which replaces the conventional matched filtering approach. We have examined the performance of this proposed CIFDM-SIC technique and compared it with the conventional CIFDM-matched filter bank and IFDM schemes. Our simulation results clearly demonstrate the superiority of the proposed scheme over the existing ones.

KEYWORDS

cyclic interleaved frequency division multiplexing, interleaved frequency division multiplexing, intersymbol interference, multipath fading, successive interference cancellation

1 | INTRODUCTION

The upcoming generation of wireless communication is expected to revolutionize cellular broadband networks, improving their capabilities across diverse domains. The developments of beyond 5G/6G will continue to enhance latency, data rate, and connectivity, introducing new technologies to achieve these purposes [1]. While 5G, the latest global standard, has made significant strides, it has become evident that it falls short of meeting future demands, particularly in terms of power and spectral efficiency [2, 3].

A comprehensive review of the challenges associated with managing radio resources for various 4G–5G dual-connectivity options as well as stand-alone networks has been presented in a recent report [4]. In response to these challenges, various multiple access (MA) schemes have been explored for potential adoption in future standards, each tailored to specific applications characterized by a distinct bit error rate (BER), signal-to-noise ratio, peak-to-average power ratio (PAPR), and complexity [5, 6]. For instance, single-carrier frequency-division multiple access (SC-FDMA), known for its PAPR, which is lower than that of orthogonal frequency-division multiple access (OFDMA), has been touted as a promising MA scheme for high-rate uplink communications [7–9].

Interleaved frequency-division multiple access (IFDMA), which stems from distributed frequency-division multiple access (DFDMA), offers better frequency diversity and performance gains than localized

frequency-division multiple access (LFDMA) and OFDMA with block allocation (B-OFDMA). IFDMA has often been viewed as a fusion of code-division multiple access (CDMA) and OFDMA [10].

To assess the suitability of IFDMA for downlink access, its error rates and PAPR have been meticulously evaluated [11]. IFDMA avoids multiple-access interference because users are allocated within orthogonal resource spaces. Nevertheless, it is exposed to intersymbol interference (ISI), and multipath fading could deteriorate its performance substantially [12, 13]. This problem has traditionally been addressed by applying well-tuned channel equalization [14].

In addition to this traditional measure, a new approach that designs the subcarrier allocation has been proposed to further enhance the ISI-combat capability efficiently [15, 16]. For instance, a bit-reversal subcarrier allocation technique was introduced in [17] to achieve flexible subcarrier allocation in IFDMA. To combat noise enhancement, hard- and soft-frequency replacement algorithms with low complexities have been developed [18]. An alternative method involving probabilistic pulse shaping and low PAPR spatial modulation has been introduced to reduce PAPR [19, 20]. To address multiple-access interference, a compensation technique was introduced based on the allocation of spreading codes to users in a block spread-IFDMA (BS-IFDMA) [21]. To enhance the BER performance and minimize channel estimation errors in the presence of ISI, a decision-directed channel estimation procedure was developed for single-user IFDMA [22].

In fact, it is now known that a property of cyclic structures can be leveraged to amplify the interference-handling performance. By capitalizing on the cyclic property of maximal length sequences (m-sequences), a cyclic interleaving structure has been embedded within code division multiplexing [23] to effectively eliminate ISI. Expanding on this, a cyclic interleaved frequency division multiplexing (CIFDM) architecture has been developed [24] and analyzed for high-data-rate transmissions [25].

This paper proposes a novel successive interference cancellation (SIC) technique for CIFDM. A comprehensive literature review underscores the significance of eliminating ISI, as emphasized by various receivers. Whereas the SIC technique traditionally serves as user detection in various MA schemes, our proposed method utilizes the unique cyclic properties of the code as a foundation for a novel multipath interference minimization process. The proposed SIC replaces the matched filter bank (MFB) presented in [24] and seamlessly integrates with CIFDM. Notably, our proposed SIC technique represents a pioneering approach to interference cancellation among existing techniques.

The remainder of the paper is structured as follows: Section 2 presents the system model with mathematical support. In Section 3, we discuss the simulation and performance analysis. The paper concludes with a discussion of the proposed work and future prospects in Section 4.

In this paper, bold letters represent vectors and matrices, and $\otimes$ represents the convolution process. The transpose and complex conjugates of a vector, scalar, or matrix are denoted by $(\cdot)^{\mathrm{T}}$ and $(\cdot)^{*}$, respectively.

2 | SYSTEM MODEL

The design of the proposed SIC technique for CIFDM is illustrated in Figure 1. In CIFDM, the user data vector, denoted as $\boldsymbol{d}$ with a length of Q, is spread using an m-sequence of length L. An m-sequence with no shift is referred to as $\boldsymbol{C}_0$, and it possesses the useful cyclic shift property for preventing an ISI. Generally, $\boldsymbol{C}_0$ with g cyclic shifts is denoted as $\boldsymbol{C}_g$. The spread data are cyclically interleaved through the following steps: First, flipping (vertically) and shifting are performed. A cyclic prefix (CP) is added to the cyclic-interleaved data to facilitate the reconstruction of the originally transmitted signal at the receiver, particularly in the presence of multipath signals. The number of CP chips placed at the start of the data frame for transmission is determined based on the channel length V. Subcarrier modulation occurs after the CP has been added and allocating a set of orthogonal frequencies to a user with a phase value of $\varphi = 2\pi/QL$.

As discussed, the data frame undergoes spreading, cyclic interleaving, CP addition, and modulation and is then transmitted over the communication channel. Let h_g represent the channel gain of a user for path g within the communication channel. Multiple copies of the

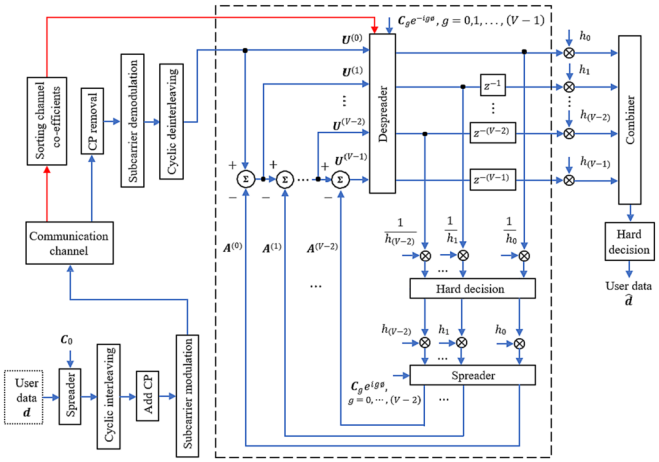

FIGURE 1 Block diagram of CIFDM using the proposed SIC technique.

transmitted data reach the receiver because of the multipath channel effect.

The user's data are detected at the receiver using the following procedure. The first step involves the removal of the added CP. Following that, the resulting signal undergoes subcarrier demodulation and subsequent cyclic deinterleaving. In the subcarrier demodulation process, the user's data are extracted by removing the assigned subcarriers. Cyclic deinterleaving is then applied to reorder the data components that were initially interleaved in a cyclic manner before transmission. We can generate V spreading codes by cyclic shifting $\boldsymbol{C}_0$ over $0, 1, \cdots, V-1$ times. The corresponding codes are used to despread the data received over each path. The multipath channel gains are sorted in descending order to sequentially detect the data from each path.

For simplicity, the channel is considered in an ordered fashion as $|h_0| > |h_1| > \cdots |h_{(V-1)}|$. Initially, $\boldsymbol{C}_0$ is used to despread the deinterleaved data with no cyclic shift, yielding the data from path 0. The data from path 0 are then multiplied by their corresponding channel gain and sent to the combiner. Simultaneously, the same despread data are divided by the channel gain, and a hard decision is applied to estimate the data for path 0. The data from path 0 are further processed by regenerating them through multiplication with the estimated data gain and spreading them with $\boldsymbol{C}_0$. This regenerated data from path 0, denoted as $\boldsymbol{A}^{(0)}$, is then subtracted from $\boldsymbol{U}^{(0)}$ (the deinterleaved data) to obtain data $\boldsymbol{U}^{(1)}$, which are subsequently despread using code $\boldsymbol{C}_1 e^{-i1\varphi}$.

The processes of despreading, estimating, and regenerating data for each specific path, followed by subtraction from the regenerated data of the previous path, are repeated until data from all available paths are obtained. The data obtained for path g are cyclically shifted g times, which is represented as z^{-g}. A final hard decision is made by combining the despread data from each path, including the required cyclic shifts, resulting in the estimated data $\widehat{\boldsymbol{d}}$ for the transmitted data $\boldsymbol{d}$.

In CIFDM, a data vector with length Q from a user is denoted as

$$\boldsymbol{d} = \left[d_0, d_1, \cdots, d_{(Q-1)}\right]. \tag{1}$$

The code used for the spreading is denoted as

$$\boldsymbol{C}_0 = \left[c_0, c_1, \cdots, c_{(L-1)}\right]^{\mathrm{T}}. \tag{2}$$

The spreading code length is the length of the data plus one. The data frame resulting from the spreading operation, followed by cyclic interleaving, has a series of symbol chips. The representation of qth symbol chip $(q = 0, 1, \cdots, Q-1)$ in the lth block $(l = 0, 1, \cdots, L-1)$ of the data frame is as follows:

$$d_q[l] = d_q c_{(q+Ql) \bmod L}. \tag{3}$$

Let V be the length of the fading channel, which is less than or equal to L. CP is used to facilitate the detection process. Therefore, $(V-1)$ data symbol chips from block $(L-1)$ are prefixed to the data frame. The CP is represented as

$$x_1(t) = \sum\nolimits_{q=Q-(V-1)}^{Q-1} d_q[L-1]\beta(t-(q-Q+V-1)T_c). \tag{4}$$

Similarly, the data frame before the CP operation is represented as

$$x_2(t) = \sum_{l=0}^{L-1}\sum_{q=0}^{Q-1} d_q[l]\beta(t-(lQ+q+V-1))T_c. \tag{5}$$

The waveform of the CP-added data frame is in the following form:

$$\begin{aligned} x_3(t) = &\sum_{q=Q-(V-1)}^{Q-1} d_q[L-1]\beta(t-(q-Q+V-1)T_c) \\ &+ \sum_{l=0}^{L-1}\sum_{q=0}^{Q-1} d_q[l]\beta(t-(lQ+q+V-1))T_c, \end{aligned} \tag{6}$$

where T_c is chip duration and $\beta(t)$ is the rectangular function. Then, $x_3(t)$ undergoes subcarrier modulation, which is processed by multiplying $e^{-ir\varphi}$, $r = 0, 1, 2, \cdots, LQ$. Therefore, the waveform representation of the data frame before transmission is represented as

$$\begin{aligned} x(t) = &\sum_{q=Q-(V-1)}^{Q-1} d_q[L-1]e^{-i(q-Q+V-1)\varphi} \\ &\times \beta(t-(q-Q+V-1)\mathrm{T}_c) \\ &+ \sum_{l=0}^{L-1}\sum_{q=0}^{Q-1} d_q[l]e^{-i(lQ+q+V-1)\varphi}\beta(t-(lQ+q+V-1))T_c, \end{aligned} \tag{7}$$

where φ is the subcarrier phase value. The transmitted data reaches the user terminal through V independent paths. The channel impulse response is

$$h(t)=\sum_{v=0}^{V-1}h_v\delta(t-\tau_v), \tag{8}$$

where h_v is vth path normalized instantaneous complex gain, τ_v is the time delay of the vth path, and $\delta(t-\tau_v)$ is the Dirac delta function. The received signal $y(t)$ at the user terminal is the sum of noise signal $n(t)$ and the convolution of transmitted signal $x(t)$ and channel impulse response $h(t)$, which is represented by the following equation:

$$y(t)=(x(t)\otimes h(t))+n(t). \tag{9}$$

First, the CP removal process is applied to the received data. The representation of qth symbol chip in the lth block of the received signal without CP is

$$y_q[l]=\sum_{v=0}^{V-1}d_{(q-v)\mathrm{mod}Q}\,c_{(q+Q(l+v))\mathrm{mod}L}\,e^{-i(q+Q(l+1)-m)\varphi}h_v(l)+n(l). \tag{10}$$

Next, the subcarrier demodulation process extracts data from the modulated carrier. The qth symbol chip representation from the lth block in the subcarrier demodulated signal is

$$\begin{aligned}u_q[l]&=y_q[l]e^{i(q+Q(l+1))\varphi}\\&=\sum_{v=0}^{V-1}d_{(q-v)\mathrm{mod}Q}\,c_{(q+Q(l+v))\mathrm{mod}L}\,e^{iv\varphi}h_v(l)\\&\quad+n(l)\,e^{i(q+Q(l+1))\varphi}.\end{aligned} \tag{11}$$

Considering a quasi-static, noise-free analysis, the above equation can be rewritten as

$$u_q[l]=\sum_{v=0}^{V-1}d_{(q-v)\mathrm{mod}Q}c_{(q+Q(l+v))\mathrm{mod}L}\,e^{iv\varphi}h_v. \tag{12}$$

2.1 | Proposed SIC technique

The proposed SIC technique aims to recover data from each path while mitigating the interference from the remaining paths. We denote the selected path as g, with a corresponding gain of h_g, where g ranges from 0 to $V-1$. These V paths are sorted in descending order based on their gain values. For simplicity, let us assume that $|h_0|>|h_1|>\cdots|h_{(V-1)}|$, making $g=0$ the dominant path. The corresponding deinterleaved data matrix with dimensions $L\times Q$ is expressed as follows:

$$\boldsymbol{U}^{(0)}=\begin{bmatrix}u_0^{(0)}[0] & u_1^{(0)}[0] & \cdots & u_{(Q-1)}^{(0)}[0]\\ u_0^{(0)}[1] & u_1^{(0)}[1] & \cdots & u_{(Q-1)}^{(0)}[1]\\ \vdots & \vdots & \vdots & \vdots\\ u_0^{(0)}[L-1] & u_1^{(0)}[L-1] & \cdots & u_{(Q-1)}^{(0)}[L-1]\end{bmatrix}. \tag{13}$$

The qth symbol in the lth block of matrix $\boldsymbol{U}^{(0)}$ is obtained by substituting $l=(l-q)/Q$ and interchanging l and q in (12), which is represented as

$$\begin{aligned}u_l^{(0)}[q]&=\sum_{v=0}^{V-1}d_{(q-v)\mathrm{mod}Q}\,c_{\left(q+Q\left(\left(\frac{l-q}{Q}\right)+v\right)\right)\mathrm{mod}L}\,e^{iv\varphi}h_v\\&=\sum_{v=0}^{V-1}d_{(q-v)\mathrm{mod}Q}c_{(l+Qv)\mathrm{mod}L}\,e^{iv\varphi}h_v.\end{aligned} \tag{14}$$

The deinterleaved matrix for an arbitrary value of $g\neq 0$ is generalized as

$$\mathbf{U}^{(g-1)}=\mathbf{U}^{(g-2)}-\mathbf{A}^{(g-2)}, \tag{15}$$

where $\mathbf{U}^{(1)}$, $\mathbf{U}^{(2)}$, $\cdots$, $\mathbf{U}^{(V-1)}$ are the matrices for the selected path $g=1, 2, \cdots, V-1$, respectively. Moreover, $\mathbf{A}^{(0)}$, $\mathbf{A}^{(1)}$, $\cdots$, $\mathbf{A}^{(V-2)}$ are the metrics associated with the selected path $g=0, 1, \cdots, V-2$, respectively. Matrix $\boldsymbol{U}^{(g)}$, with dimensions $L\times Q$ for path $g\neq 0$, can be defined as

$$\mathbf{U}^{(g)}=\begin{bmatrix}u_0^{(g)}[0] & u_0^{(g)}[1] & \cdots & u_0^{(g)}[Q-1]\\ u_1^{(g)}[0] & u_1^{(g)}[1] & \cdots & u_1^{(g)}[Q-1]\\ \vdots & \vdots & \vdots & \vdots\\ u_{L-1}^{(g)}[0] & u_{L-1}^{(g)}[1] & \cdots & u_{(L-1)}^{(g)}[Q-1]\end{bmatrix}. \tag{16}$$

The qth symbol in the lth block of matrix $\mathbf{U}^{(g)}$ for $g\neq 0$ is obtained by

$$u_l^{(g)}[q]=u_l^{(g-1)}[q]-a_l^{(g-1)}[q]. \tag{17}$$

Here, $a_l^{(g-1)}[q]$ represents qth symbol in the lth block of matrix $\mathbf{A}^{(g-1)}$ for path $(g-1)$. Similarly, matrix $\mathbf{A}^{(g)}$, with dimensions $L\times Q$ for path $g\neq V-1$, can be defined as

$$\mathbf{A}^{(g)} = \begin{bmatrix} a_0^{(g)}[0] & a_0^{(g)}[1] & \cdots & a_0^{(g)}[Q-1] \\ a_1^{(g)}[0] & a_1^{(g)}[1] & \cdots & a_1^{(g)}[Q-1] \\ \vdots & \vdots & \vdots & \vdots \\ a_{L-1}^{(g)}[0] & a_{L-1}^{(g)}[1] & \cdots & a_{L-1}^{(g)}[Q-1] \end{bmatrix}. \quad (18)$$

The qth symbol in the lth block of $\mathbf{A}^{(g)}$ for $g = 0, 1, \cdots, V-2$ is determined by

$$a_l^{(g)}[q] = h_g \widehat{d}_q\{g\} c_{(l+Qg)\mathrm{mod}L} e^{ig\varphi}. \quad (19)$$

The despread data vector $\mathbf{d}\{0\}$ for path $g = 0$ is obtained by despreading matrix $\mathbf{U}^{(0)}$ with $\mathbf{C}_0 e^{-i0\varphi}$. The qth symbol of despread data $\mathbf{d}\{0\}$ is

$$d_q\{0\} = \sum_{l=0}^{L-1} u_l^{(0)}[q] c_{l\mathrm{mod}L} e^{-i0\varphi}. \quad (20)$$

Using (14), we can write

$$\begin{aligned} d_q\{0\} &= \sum_{l=0}^{L-1} \left(\sum_{v=0}^{V-1} d_{(q-v)modQ} c_{(l+Qv)\mathrm{mod}L} e^{iv\varphi} h_v \right) c_{l\mathrm{mod}L} \\ &= \sum_{l=0}^{L-1} d_{(q)\mathrm{mod}Q} c_{l\mathrm{mod}L}^2 h_0 \\ &+ \sum_{v=1}^{V-1} \sum_{l=1}^{L-1} d_{(q-v)\mathrm{mod}Q} c_{(l+Qv)\mathrm{mod}L} c_{l\mathrm{mod}L} e^{iv\varphi} h_v \end{aligned} \quad (21)$$

Using correlation properties, we can write $\sum_{l=0}^{L-1} c_{l\mathrm{mod}L}^2 = 1$ and $\sum_{l=0}^{L-1} c_{(l+Qv)\mathrm{mod}L} c_{l\mathrm{mod}L} = 0$.
Therefore, (21) becomes

$$d_q\{0\} = d_q h_0 \quad (22)$$

By analyzing (22), the generalized equation for the qth symbol of despread data for $g = 0, 1, \cdots, V-1$ is

$$d_q\{g\} = d_{(q-g)\mathrm{mod}Q} h_g. \quad (23)$$

The despread data vector $\mathbf{d}\{g\}$ with dimensions $1 \times Q$ takes the following form:

$$\mathbf{d}\{g\} = \left[d_0\{g\}, d_1\{g\}, \cdots, d_{(Q-1)}\{g\} \right]. \quad (24)$$

The estimate of the qth symbol of despread data $d_q\{g\}$ is obtained by applying the hard decision to (23), which yields

$$\widehat{d}_q\{g\} = \mathrm{sgn}\left\{ \frac{d_q\{g\}}{h_g} \right\} = d_{(q-g)\mathrm{mod}Q}. \quad (25)$$

Furthermore, vector $\widehat{\mathbf{d}}\{g\}$ with dimensions $1 \times Q$ will be in the following form:

$$\widehat{\mathbf{d}}\{g\} = \left[\widehat{d}_0\{g\}, \widehat{d}_1\{g\}, \cdots, \widehat{d}_{(Q-1)}\{g\} \right] \quad (26)$$

Substituting (25) into (19), we get

$$a_l^{(g)}[q] = h_g d_{(q-g)\mathrm{mod}Q} c_{(l+Qg)\mathrm{mod}L} e^{ig\varphi} \quad (27)$$

Using (14), (17), and (27), the expression for $g = 1$ can be written as

$$\begin{aligned} u_l^{(1)}[q] &= u_l^{(0)}[q] - a_l^{(0)}[q] \\ &= \left(\sum_{v=0}^{V-1} d_{(q-v)\mathrm{mod}Q} c_{(l+Qv)\mathrm{mod}L} e^{iv\varphi} h_v \right) \\ &\quad - \left(h_0 d_{(q-0)\mathrm{mod}Q} c_{(l+Q(0))\mathrm{mod}L} e^{i0\varphi} \right) \\ &= \left(\sum_{v=1}^{V-1} d_{(q-v)\mathrm{mod}Q} c_{(l+Qv)\mathrm{mod}L} e^{iv\varphi} h_v \right) \end{aligned} \quad (28)$$

By analyzing (28), the generalized equation for the qth symbol in the lth block of matrix $\mathbf{U}^{(g)}$ for $g \neq 0$ is obtained as

$$u_l^{(g)}[q] = \sum_{v=g}^{V-1} d_{(q-v)\mathrm{mod}Q} c_{(l+Qv)\mathrm{mod}L} e^{iv\varphi} h_v. \quad (29)$$

As a result, the multipath components become resolvable owing to their orthogonality, resulting from the cyclic interleaving combined with the proposed SIC. The following subsections discuss various methods of combining these multipath components.

2.1.1 | Linear combiner

The substitution of $q+g$ for the qth symbol in $d_q\{g\}$ represents a cyclic shift. The cyclically shifted elements are combined using LC as follows:

$$D_{q,LC} = \sum_{g=0}^{V-1} d_{(q+g)}\{g\}. \quad (30)$$

Using (23), we can rewrite (30) as

$$D_{q,LC} = \sum_{g=0}^{V-1} d_{q\bmod Q} h_g = d_q \sum_{g=0}^{V-1} h_g. \tag{31}$$

The hard decision applied to the combined output yields

$$\widehat{d}_{q,\mathrm{LC}} = \mathrm{sgn}\{D_{q,\mathrm{LC}}\} = sgn\left\{d_q \sum_{g=0}^{V-1} h_g\right\}. \tag{32}$$

The estimated user data obtained from LC is of the form

$$\widehat{\boldsymbol{d}}_{LC} = \left[\widehat{d}_{0,LC}, \widehat{d}_{1,LC}, \cdots \widehat{d}_{(Q-1),LC}\right]. \tag{33}$$

2.1.2 | Maximal ratio combiner

Replacing q with $q+g$ followed by MRC yields the qth symbol as follows:

$$D_{q,\mathrm{MRC}} = \sum_{g=0}^{V-1} d_{q+g}\{g\} h_g^*. \tag{34}$$

Rewriting (34) with (23) gives

$$D_{q,\mathrm{MRC}} = \sum_{g=0}^{V-1} d_{(q)\bmod Q} h_g h_g^* = d_q \sum_{g=0}^{V-1} |h_g|^2. \tag{35}$$

The estimate of the qth symbol from the MRC is written as follows:

$$\widehat{d}_{q,\mathrm{MRC}} = \mathrm{sgn}\{D_{q,\mathrm{MRC}}\} = \mathrm{sgn}\left\{d_q \sum_{g=0}^{V-1} |h_g|^2\right\}. \tag{36}$$

Consequently, the MRC output in vector form is

$$\widehat{\mathbf{d}}_{\mathrm{MRC}} = \left[\widehat{d}_{0,\mathrm{MRC}}, \widehat{d}_{1,\mathrm{MRC}}, \cdots, \widehat{d}_{(Q-1),\mathrm{MRC}}\right]. \tag{37}$$

The proposed SIC technique for CIFDM enhances the receiver's ability to resolve and combine multipath-scattered components. Specifically, this technique eliminates the most significant interfering paths in successive path detections. The subsequent sections provide a detailed process flow and simulations to support the mathematical derivations.

2.2 | Process diagram 1

Figure 2 illustrates the transmission and reception of data vectors in CIFDM. In this illustration, we assume CIFDM symbol transmission with $Q=3$, $L=4$, and $V=2$. The transpose of the code vector, with a size of $L \times 1$, spreads the data vector, which has a size of $1 \times Q$. Consequently, the resulting spread data dimensions are $L \times Q$. To create cyclic interleaved data with the same $L \times Q$ dimensions, we flip the data components of the spread data vertically and apply cyclic shifts ranging from 0 to $Q-1$ to each of the columns. A data frame is constructed with a size of $1 \times LQ$ by reading the cyclic interleaved data rowwise. By adding a CP of size $V-1$ at the beginning of the frame, its final size becomes $1 \times ((V-1)+LQ)$. The subcarrier-modulated data are then transmitted over the multipath channel.

Upon receiving the data and removing the CP, it returns to its original size before the addition of the CP. When we reverse the reshaping process on the subcarrier-demodulated data, the resulting data maintains the size and format as the cyclic interleaved data. Furthermore, performing cyclic deinterleaving on the reshaped data leads to data with the same size and format as the spread data. The output data vector, obtained by applying the proposed SIC technique, combining, and making a hard decision on the deinterleaved data, has the same size as the transmitted data vector, which is $1 \times Q$.

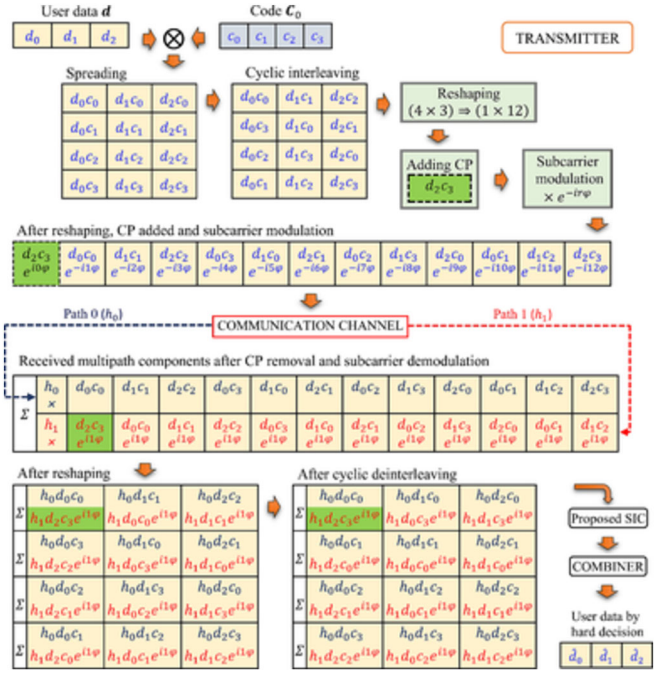

FIGURE 2 Processes on a data vector in CIFDM with $Q=3$, $L=4$, and $V=2$.

2.3 | Process diagram 2

Figure 3 provides an illustration of the proposed SIC technique in CIFDM with $Q=3$, $L=4$, and $V=2$. The SIC technique commences with the deinterleaving process. The deinterleaved data, originally with dimensions $L\times Q$, are transformed into a $1\times Q$ format by despreading them with $\boldsymbol{C}_0$. The estimated data for path 0 are then spread again using $\boldsymbol{C}_0$ to match the dimensions of the deinterleaved data. This spreading operation facilitates the subsequent matrix subtraction. To obtain data for path 1 with dimensions $1\times Q$, we perform despreading on the output of the subtraction using $\boldsymbol{C}_1 e^{-i1\varphi}$. The despread data per path, combined output from either LC or MRC, and detected user data have dimensions $1\times Q$.

2.4 | Flow chart

Figure 4 shows a flowchart illustrating the operation of the proposed SIC receiver in CIFDM. The flowchart starts with the reception of multipath components from a fading channel. The SIC technique begins by arranging the channel values in descending order of channel gain, making the following assumption: $|h_0|>|h_1|>\cdots|h_{(V-1)}|$. Initialization involves setting both the selected path and combined output to 0. The data acquisition process is successively repeated $V-1$ times. The data regeneration process is consecutively repeated $V-2$ times.

Both the IFDM and CIFDM schemes require channel state information (CSI) at the receiver for channel equalization. Specifically, the proposed CIFDM-SIC requires the CSI at both the SIC and MRC stages, CIFDM-MFB only at the MRC stage, and IFDM at the minimum mean square error frequency domain equalization (MMSE-FDE) stage. Consequently, the complexity of IFDM is slightly higher than that of CIFDM-MFB [25].

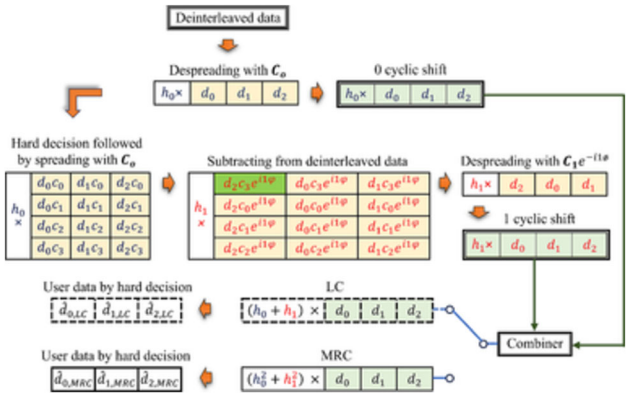

FIGURE 3 Process of proposed SIC technique in CIFDM with $Q=3, L=4$, and $V=2$.

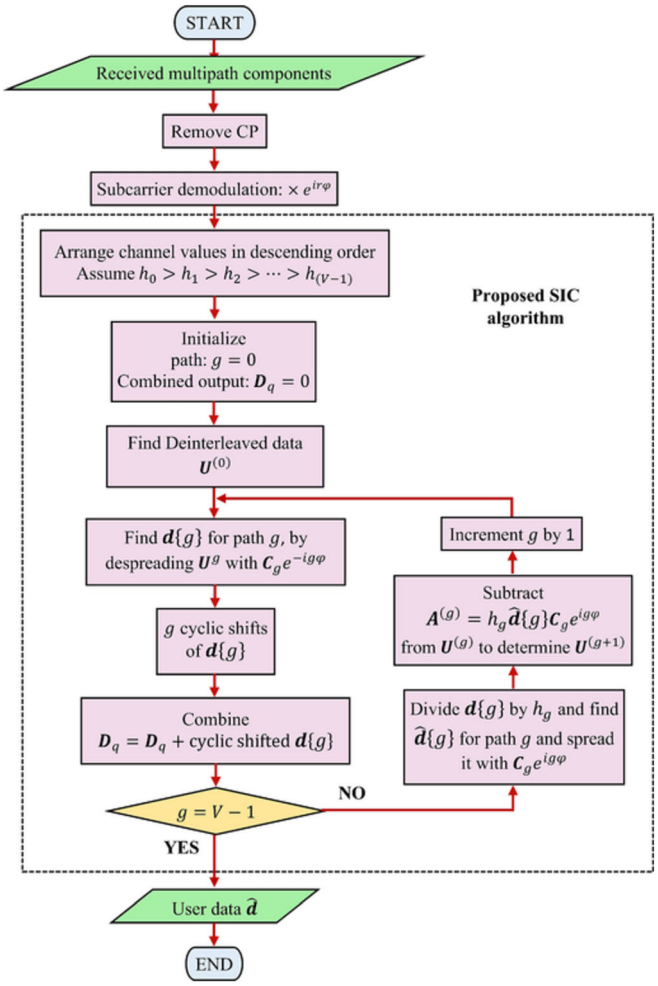

FIGURE 4 Flow chart for the proposed technique.

In CIFDM schemes, the performance improvement depends on an increased number of significant paths. The multipath resolution achieved using the proposed CIFDM-SIC is remarkable compared with that of CIFDM-MFB, albeit at a moderate increase in system complexity. However, this slight increase in complexity in the proposed CIFDM-SIC is justifiable, given the substantial diversity gain it provides.

3 | SIMULATION

The BER performance of the CIFDM with the proposed SIC and MFB receivers and IFDM with the MMSE-FDE receiver were evaluated using Monte Carlo simulations. The comparative curves based on channels, combiners, magnitude of interference between users, and imperfect channel estimates are presented in this section to demonstrate the remarkable performance of the proposed CIFDM-SIC. Binary phase-shift keying (BPSK) modulation without pulse shaping was considered. The

amplitude profile of the multipath channel was created based on the energy levels of line of sight (LoS) and scattered components. The Rician factor is the average energy ratio of the LoS to the scattered components. A performance analysis was performed under both LoS and non-line-of-sight (NLoS) channels.

Figure 5 shows the advantages of the proposed CIFDM-SIC over IFDM under different channel conditions, characterized by Rician factors of 100 dB (strong LoS), −20 dB (weak LoS), and −100 dB (NLoS). We employed the proposed SIC receiver for CIFDM and MMSE-FDE for IFDM. To validate the multipath simulations for both schemes, we used a 100 dB channel in which they performed similarly. However, a substantial performance gap emerged between the two schemes when applied to the other two channels, highlighting the superiority of CIFDM-SIC in multipath fading scenarios. This performance gap is attributed to the absence of the cyclic interleaving technique in IFDM, resulting in a lower diversity gain.

The conventional scheme outperformed the others in the 100 dB channel because of its strong LoS and the absence of scattered components. It maintained a marginal performance gap in the −20 dB channel when compared with the 100 dB channel because of the weak LoS and presence of scattered components. Conversely, the worst performance, obtained in the −100 dB channel, was expected, given its NLoS nature.

The proposed CIFDM-SIC excelled in the −20 dB and −100 dB channels because of its multipath resolution capability. However, unlike IFDM, the proposed scheme responded differently in the various channels considered. It exhibited poor performance in the 100 dB channel owing to the absence of scattered components, whereas its superior performance in the −20 dB channel was attributed to both the weak LoS and scattered components. Similarly, the −100 dB channel performed worse than the −20 dB channel due to its NLoS characteristics. For subsequent simulations, we assumed the −100 dB channel to maintain realism.

Figure 6 presents the remarkable robustness of the proposed scheme against multipath fading and its substantial improvement in diversity compared with CIFDM-MFB, as described in [24]. Since CIFDM-MFB does not employ a multistage multipath interference minimization technique, its performance is marginally inferior to that of the proposed scheme. Furthermore, IFDM maintains a significant performance gap with both CIFDM schemes owing to the absence of any multipath resolution strategy.

Figure 7 presents the BER performance of CIFDM for both the proposed SIC and MFB receivers, utilizing LC and MRC across varying code lengths. The code lengths considered for the comparison were $L = 7$, 15, 31, and 63. We compared the E_b/N_0 values of different cases at a fixed BER of 10^{-6}.

It is evident that the proposed CIFDM-SIC outperformed CIFDM-MFB in all eight cases. Notably, there is a significant performance improvement in both schemes when transitioning from $L = 7$ to $L = 63$. Furthermore, as the code length increased from 7 to 63, the performance of CIFDM-MFB gradually approached that of the proposed scheme.

Overall, there was a substantial performance improvement when MRC was used instead of LC. Additionally, the performance of MRC was excellent

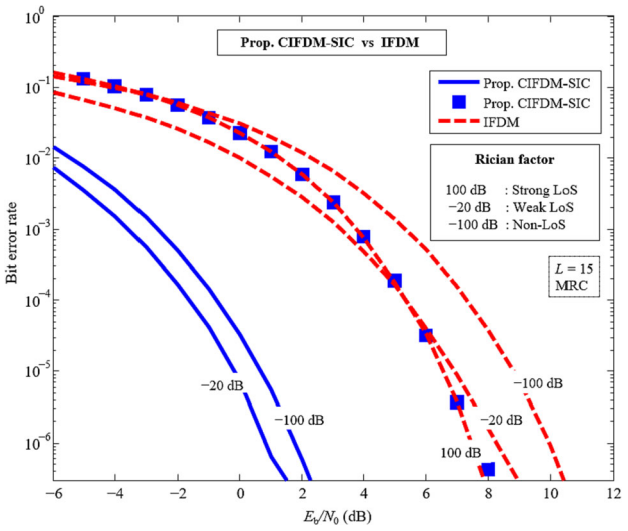

FIGURE 5 BER performance comparison of proposed CIFDM-SIC and IFDM for various Rician factors.

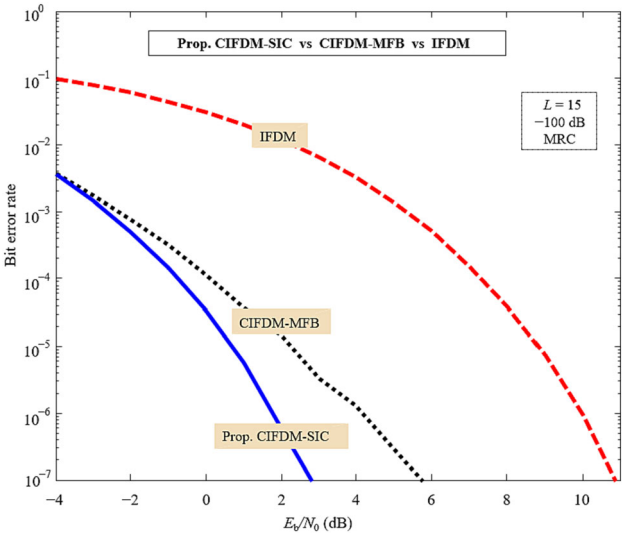

FIGURE 6 BER performance comparison of the proposed CIFDM-SIC, CIFDM-MFB, and IFDM.

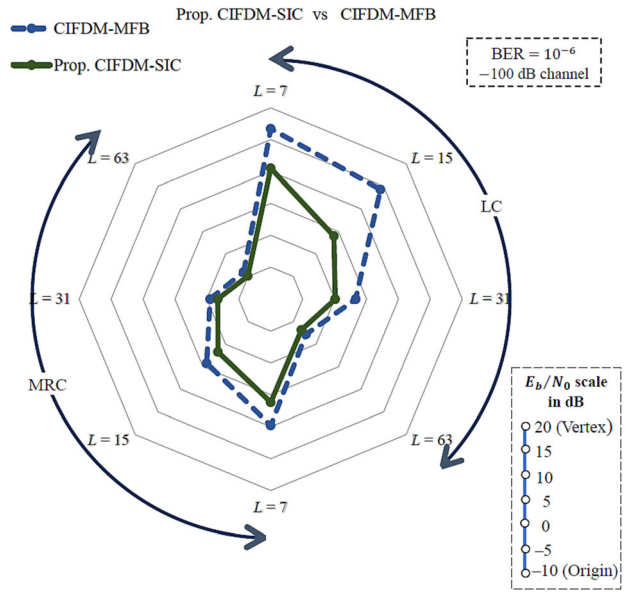

FIGURE 7 Spider plot of CIFDM for various detectors, combiners, and code lengths at a specific BER of 10^{-6}.

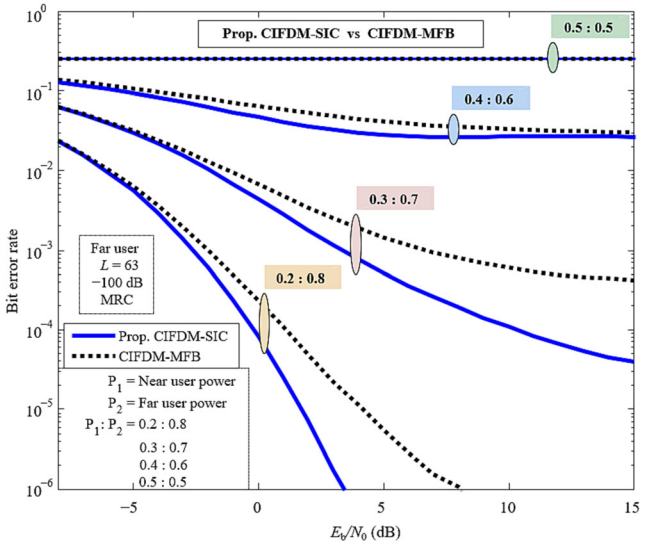

FIGURE 8 BER comparison of the proposed CIFDM-SIC and CIFDM-MFB under MA scenarios and different magnitudes of interference between users.

when $L = 63$, leading us to select MRC with $L = 63$ for the remainder of the analysis.

Figure 8 shows the proposed CIFDM-SIC and CIFDM-MFB under a non-orthogonal multiple access (NOMA) scenario. The performance was studied for a two-user NOMA cluster with different levels of interference affecting the desired far user. Assuming extreme and distinct channel conditions for the two users, we considered a −100 dB (poor channel) for the far user and a 20 dB (good channel) for the near user. The magnitude of interfering power was varied from 0.2 to 0.5 in increments of 0.1, with the sum of interfering and desired user's power assumed to be equal to one.

In conventional NOMA, SIC is a standard detector for the near user but not for the far user. However, since the proposed CIFDM-SIC demonstrates exceptional performance for the −100 dB channel, as shown in Figure 5, it is also employed for the far user in the proposed NOMA transmission. It is important to note that the SIC techniques used for the near and far users are entirely different, particularly in terms of how they resolve multiple paths. The far user benefits from multipath resolution; however, this is not the case for the near user.

The observations show a consistent error trend at a near- and far-user power ratio of 0.5:0.5. However, the performance continued to improve as the interference power gradually reduced. Both schemes performed exceptionally well at a power ratio of 0.2:0.8. However, CIFDM-MFB lagged behind CIFDM-SIC in this scenario. Therefore, we assumed a power ratio of 0.2:0.8 for the subsequent performance analysis.

As it is often challenging to obtain a perfect CSI estimate in real-world scenarios, our simulation setup accounts for the practicality of imperfect CSI, as shown in Figure 9. In our evaluation, we compared the performance of the proposed and conventional schemes under a −100 dB channel condition, considering a near–far user power ratio of 0.2:0.8.

We modeled the imperfect channel estimate as $\widehat{h}_g = h_g + \omega\alpha$, where h_g represents the ideal channel, ω^2 denotes the normalized mean square error (NMSE), and α is a Gaussian random variable with a mean of 0 and variance of 1. The NMSE for the channel estimate is calculated as

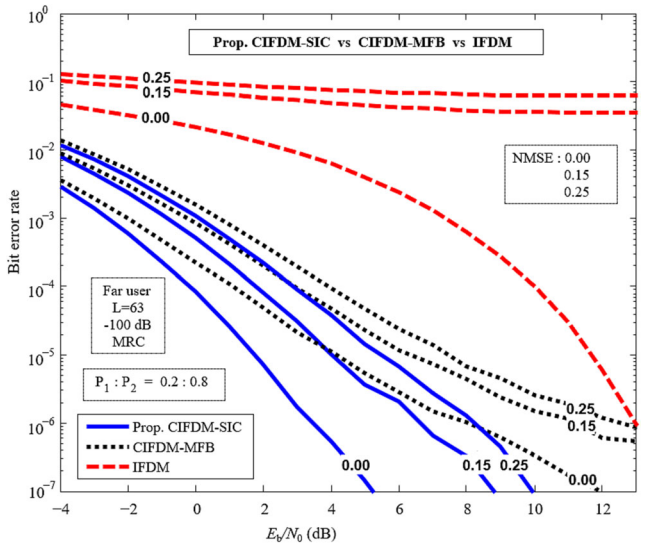

FIGURE 9 Effect of imperfect channel estimation in BER performance of the far user for the proposed CIFDM-SIC, CIFDM-MFB, and IFDM.

$$\omega^2 = E\left\{\left|h_g - \widehat{h}_g\right|^2\right\} / E\left\{\left|h_g\right|^2\right\}. \quad (38)$$

In our analysis, we present the performance curves for different NMSE values ranging from 0 to 0.25. Notably, the BER performance of the conventional IFDM scheme was found to be the poorest. However, our proposed scheme outperformed conventional approaches, even in scenarios with higher NMSE levels.

4 | CONCLUSION

This paper introduced a novel multistage multipath interference cancellation technique for CIFDM. The user performance in data transmission over a weak communication channel is significantly enhanced by the proposed CIFDM-SIC. The proposed scheme offers advantages such as diversity in reception, and eliminates the need for MMSE-FDE equalization. We conducted a comprehensive analysis, examining the error rates across various code lengths, receivers, and combiners. The simulation results clearly indicate that our proposed scheme significantly improves performance compared with the conventional CIFDM-MFB and IFDM approaches. Additionally, we demonstrate robustness in MA and imperfect channel estimation scenarios. A promising future direction for our research is to extend this work by developing advanced multistage interference minimization techniques for CIFDM.

CONFLICT OF INTEREST STATEMENT

The author declares that there are no conflicts of interest.

ORCID

S. Lenty Stuwart https://orcid.org/0000-0002-9988-5624

REFERENCES

1. A. Dogra, R. K. Jha, and S. Jain, *A survey on beyond 5G network with the advent of 6G: architecture and emerging technologies*, IEEE Access **9** (2021), 67512–67547.
2. Z. E. Ankarali, B. Peköz, and H. Arslan, *Flexible radio access beyond 5G: a future projection on waveform, numerology, and frame design principles*, IEEE Access **5** (2017), 18295–18309.
3. C. -X. Wang, X. You, X. Gao, X. Zhu, Z. Li, C. Zhang, H. Wang, Y. Huang, Y. Chen, H. Haas, J. S. Thompson, E. G. Larsson, M. Di Renzo, W. Tong, P. Zhu, X. Shen, H. V. Poor, and L. Hanzo, *On the road to 6G: visions, requirements, key technologies, and testbeds*, IEEE Commun. Surv. Tutor. **25** (2023), no. 2, 905–974.
4. M. Agiwal, H. Kwon, S. Park, and H. Jin, *A survey on 4G–5G dual connectivity: road to 5G implementation*, IEEE Access **9** (2021), 16193–16210.
5. A. F. M. S. Shah, A. N. Qasim, M. A. Karabulut, H. Ilhan, and M. B. Islam, *Survey and performance evaluation of multiple access schemes for next-generation wireless communication systems*, IEEE Access **9** (2021), 113428–113442.
6. T. Kebede, Y. Wondie, J. Steinbrunn, H. B. Kassa, and K. T. Kornegay, *Multi-carrier waveforms and multiple access strategies in wireless networks: performance, applications, and challenges*, IEEE Access **10** (2022), 21120–21140.
7. H. G. Myung, J. Lim, and D. J. Goodman, *Single carrier FDMA for uplink wireless transmission*, IEEE Veh. Technol. Mag. **1** (2006), no. 3, 30–38.
8. S. P. Yadav and S. C. Bera, Single carrier FDMA technique for wireless communication system, (Proc. Conf. 2015 Annual IEEE India Conference (INDICON), New Delhi, India), 2015, pp. 1–6.
9. R. Saadia and N. M. Khan, *Single carrier-frequency division multiple access radar: waveform design and analysis*, IEEE Access **8** (2020), 35742–35751.
10. T. Frank, A. Klein, and E. Costa, *IFDMA: a scheme combining the advantages of OFDMA and CDMA*, IEEE Wirel. Commun. **14** (2007), no. 3, 9–17.
11. O. Takyu and M. Nakagawa, IFDM for downlink wireless access scheme and performance comparison to MC-CDM, (Proc. Conf. 2007 IEEE 18th International Symposium on Personal, Indoor and Mobile Radio Communications, Athens, Greece), 2007, pp. 1–5.
12. T. -H. Pham, Y. -C. Liang, and A. Nallanathan, *A joint channel estimation and data detection receiver for multiuser MIMO IFDMA systems*, IEEE Trans. Commun. **57** (2009), no. 6, 1857–1865.
13. O. Takyu and M. Nakagawa, Frequency spectrum rotation in interleaved frequency division multiplexing, (Proc. Conf. IEEE GLOBECOM 2007 – IEEE Global Telecommunications Conference, Washington, DC, USA), 2007, 4543–4547.
14. H. Qu, G. Liu, Y. Wang, Q. Chen, C. Yi, and J. Peng, *A time-domain approach to channel estimation and equalization for the SC-FDM system*, IEEE Trans. Broadcast. **65** (2019), no. 4, 713–726.
15. S. Kumar, M. S. Chaudhari, R. Gupta, and S. Majhi, *Multiple CFOs estimation and implementation of SC-FDMA uplink system using oversampling and iterative method*, IEEE Trans. Veh. Technol. **69** (2020), no. 6, 6254–6263.
16. S. C. Liew and Y. Shao, *New transceiver designs for interleaved frequency-division multiple access*, IEEE Trans. Wirel. Commun. **19** (2020), no. 12, 7765–7778.
17. Y. Shao and S. C. Liew, *Flexible subcarrier allocation for interleaved frequency division multiple access*, IEEE Trans. Wirel. Commun. **19** (2020), no. 11, 7139–7152.
18. D. Kim, H. -M. Kim, and G. -H. Im, *Iterative channel estimation with frequency replacement for SC-FDMA systems*, IEEE Trans. Commun. **60** (2012), no. 7, 1877–1888.
19. J. Ji, G. Ren, and H. Zhang, *PAPR reduction of SC-FDMA signals via probabilistic pulse shaping*, IEEE Trans. Veh. Technol. **64** (2015), no. 9, 3999–4008.
20. D. Sinanović, G. Šišul, and B. Modlic, *Low-PAPR spatial modulation for SC-FDMA*, IEEE Trans. Veh. Technol. **66** (2017), no. 1, 443–454.
21. K. -B. Png, X. Peng, F. Chin, and C. C. Ko, *Mobility-based interference cancellation scheme for BS-IFDMA systems with*

optimum code assignment, IEEE Trans. Veh. Technol. **62** (2013), no. 5, 2105–2117.
22. W. Li, O. Takyu, K. Adachi, and M. Nakagawa, Performance evaluation of decision directed channel estimation for single user IFDMA, (Proc. Conf. 2008 IEEE Radio and Wireless Symposium, Orlando, FL, USA), 2008, pp. 659–662.
23. S. L. Stuwart and T. Selvi, *Zero intersymbol interference multi-user system: a new architecture utilising m-sequence cyclic property*, IET Commun. **9** (2015), no. 15, 1924–1931.
24. J. A. Kumar and S. L. Stuwart, *Cyclic interleaving scheme for an IFDMA system*, Ann. Telecommun. **75** (2020), no. 5–6, 241–252.
25. J. A. Kumar and S. L. Stuwart, *Intersymbol interference resilient interleaving architecture for multi-stream interleaved frequency division multiple access system*, Int. J. Commun. Sys. **63** (2023), 1–21.

AUTHOR BIOGRAPHIES

G. Anuthirsha received her bachelor's degree in electronics and communication engineering from Alagappa Chettiar College of Engineering and Technology, Karaikudi, India, in 2013, and her master's degree in applied electronics from the Regional Centre of Anna University, Tirunelveli, India, in 2015. Presently, she is doing her full-time doctoral research at the University College of Engineering, Nagercoil, India. Her main research interests are wireless communication, digital signal processing, and digital communication.

S. Lenty Stuwart earned his bachelor's degree in electronics and communication engineering in 2001 from Manonmaniam Sundaranar University, Tirunelveli, India, and a Master of Technology degree in digital systems and communication engineering in 2006 from the National Institute of Technology, Calicut, India. He conducted his doctoral research at Anna University, India. Currently, he serves as an Assistant Professor and Head of the Department of ECE at the University College of Engineering, Nagercoil. He is a recipient of an Early Career Research Award. He currently guides research work in wireless sensor communication, digital modulation, and signal processing.

How to cite this article: G. Anuthirsha and S. L. Stuwart, *Multistage interference cancellation for cyclic interleaved frequency division multiplexing*, ETRI Journal **46** (2024), 904–914. DOI 10.4218/etrij.2023-0274.